

# Direct Detection of the Ultrafast Response of Charges and Molecules in the Photoinduced Neutral-to-Ionic Transition of the Organic Tetrathiafulvalene-*p*-Chloranil Solid

H. Uemura<sup>1</sup> and H. Okamoto<sup>1,2</sup>

<sup>1</sup>Department of Advanced Materials Science, University of Tokyo, Chiba 277-8561, Japan

<sup>2</sup>CREST, Japan Science and Technology Agency (JST), Tokyo 102-0075, Japan

(Received 30 June 2010; published 16 December 2010)

Ultrafast dynamics of charge and molecular degrees of freedom in a photoinduced neutral-ionic transition of an organic solid, tetrathiafulvalene-*p*-chloranil, were directly detected for the first time by transient reflectivity measurements using 15 fs laser pulses. The results reveal that ionic domains are photogenerated in the neutral lattice via collective charge-transfer processes within 20 fs, and subsequently molecular deformations and bendings occur, giving rise to large changes in the molecular ionicity and charge redistributions in molecules, respectively. We show that such couplings between charge and molecular degrees of freedom play important roles in photoinduced transitions of organic molecular compounds.

DOI: 10.1103/PhysRevLett.105.258302

PACS numbers: 82.53.Xa, 71.38.-k, 73.20.Mf, 78.47.jg

Photo control of an electronic phase in solids, which is called photoinduced phase transition (PIPT), is attracting much attention [1]. A key strategy for the realization of an ultrafast PIPT is to irradiate a material located near a boundary between two phases having different electronic structures with a femtosecond (fs) laser pulse. Organic molecular compounds are good target materials, since some compounds include strong instabilities originating from both electron correlations and couplings between charge and molecular or lattice degrees of freedom, and show characteristic phase transitions by lowering temperature and/or applying pressure. A photoexcitation can stimulate such instabilities and ultrafast PIPTs are expected to be driven.

A typical example of PIPTs in organic molecular compounds is a photoinduced neutral-to-ionic (*NI*) transition observed in tetrathiafulvalene (TTF)-*p*-chloranil (CA) [2–4]. By lowering temperature, TTF-CA shows the *NI* transition at 81 K [5], which is accompanied by the changes of molecular ionicity and the changes of structures, intramolecular (IM) deformations as well as lattice displacements [6]. In the photoinduced *NI* transition, however, dynamics of charge and molecular degrees of freedom were not detected due to the lack of the time resolution in the previous studies. In this study, by the pump-probe (PP) measurements using 15 fs laser pulses, we have detected ultrafast charge and IM deformation dynamics for the first time.

TTF-CA is a molecular (DA) compound, which consists of alternately stacked  $\pi$ -electron donor *D* (TTF) and acceptor *A* (CA) molecules [Fig. 1(a)] [7]. In DA compounds, there are two phases, a neutral (*N*) phase and an ionic (*I*) phase. An *I* phase is stabilized when the long-range Coulomb attractive energy for a DA pair in *I* molecular stacks overcomes its ionization energy [7]. Because of the overlap of  $\pi$  orbitals between *D* and *A*, the degree of the charge-transfer (CT)  $\rho$  from *D* to *A* is not equal to

0 or 1. In TTF-CA,  $\rho \sim 0.3$  in the *N* phase and  $\sim 0.7$  in the *I* phase [8]. In the *I* phase, the DA molecules are dimerized due to the spin-Peierls mechanism [6]. The *NI* transition can also be driven by photoirradiation [3,4]. The transfer energy  $t_{DA}$  ( $\sim 0.2$  eV) and the frequencies of the IM vibration modes ( $\sim 300$ – $1500$   $\text{cm}^{-1}$ ) correspond to time scales

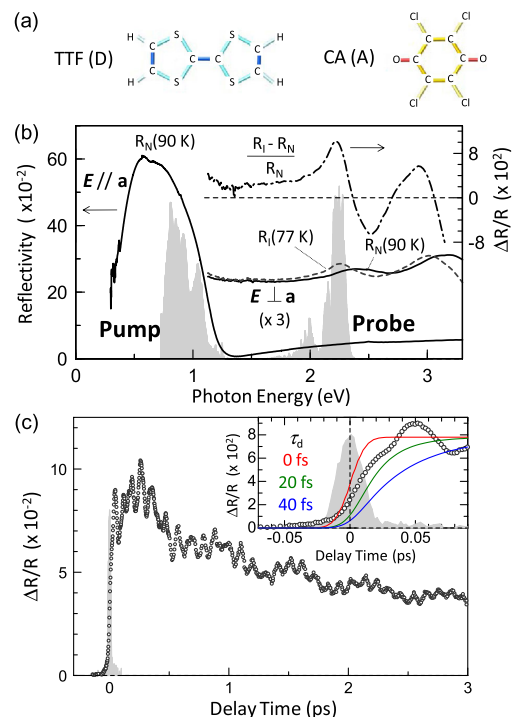


FIG. 1 (color online). (a) Molecular structures of TTF-CA. (b) Reflectivity ( $R$ ) spectra in the *N* phase ( $R_N$ ) and *I* phase ( $R_I$ ) and a differential  $R$  spectrum  $[(R_I - R_N)/R_N]$ . Spectral profiles of pump and probe pulses are also shown. (c) Time characteristic of photoinduced  $R$  changes ( $\Delta R/R$ ). Gray shades show a cross-correlation profile of pump and probe pulse. Solid lines in the inset are simulated time characteristics.

of  $\sim 20$  fs and  $\sim 100 - 20$  fs, respectively [9–11]. Therefore, to detect the charge and molecular dynamics, the duration of the laser pulse should be less than 20 fs. In the present study, we performed PP measurements using 15 fs laser pulses.

Single crystals of TTF-CA were grown by the cosublimation method [4]. In the PP measurements, the pump and probe pulses were provided by two noncollinear optical parametric amplifiers, both of which were excited with an output of a Ti:sapphire regenerative amplifier (795 nm, a duration of 130 fs, and a repetition of 1 kHz). The pulse widths were 15 fs. The system response was determined by the cross correlation between the pump and probe pulses using a  $\beta$ -BaB<sub>2</sub>O<sub>4</sub> crystal. The excitation photon density  $x_{\text{ph}}$  is defined as the averaged photon density per pump pulse absorbed within its absorption depth  $l_p$  (the inverse of the absorption coefficient) and evaluated from  $x_{\text{ph}} = I_p(1 - R_p)(1 - 1/e)/l_p$ , where,  $I_p$ , and  $R_p$  are the photon density per unit area and the reflection loss of the pump light, respectively.

In Fig. 1(b), we show the polarized reflectivity ( $R$ ) spectra,  $R_N$  in the  $N$  phase (90 K) and  $R_I$  in the  $I$  phase (77 K), together with the spectral profiles of the pump and probe pulses (gray shades). The strong band at  $\sim 0.6$  eV polarized parallel ( $//$ ) to the stacking axis  $\mathbf{a}$  is due to the CT band between the  $D$  and  $A$  molecules. The pump pulse is set at the CT band. For a probe of the  $NI$  transition dynamics, i.e., changes in  $\rho$ , we focus on the IM transition band of TTF at  $\sim 2$  eV polarized perpendicular ( $\perp$ ) to  $\mathbf{a}$ . The energy position and intensity of the band depend strongly on  $\rho$  [4]. In Fig. 1(b), we also show the differential  $R$  spectrum  $(R_I - R_N)/R_N$ , which exhibits a clear peak at 2.25 eV. By probing the photoinduced reflectivity changes  $\Delta R/R$  at 2.25 eV, the  $NI$  transition can be detected. The gray shade in the inset of Fig. 1(c) shows a cross correlation of a pump and a probe pulse. The temporal width  $\sim 20$  fs corresponds to the time resolution.

The time characteristic of  $\Delta R/R$  measured with  $x_{\text{ph}}$  of  $0.07 \pm 0.01$  photons/DA at 90 K as a function of the delay time  $t_d$  is shown in Fig. 1(c). The positive signal indicates the photogeneration of an  $I$  state. By comparing the magnitude of the signal to  $(R_I - R_N)/R_N$ , we deduce that an  $I$  state generated by one photon consists of  $\sim 10$  DA pairs and 70% of the  $N$  states are converted to the  $I$  states. First, we discuss the rise time  $\tau$  of  $\Delta R/R$ . The solid lines in the inset of Fig. 1(c) show simulated time profiles for  $\tau = 0, 20,$  and  $40$  fs. A comparison of the experimental and simulated time profiles reveals that the characteristic time for the  $I$ -domain formation is  $\leq 20$  fs. The time scale of the CT processes deduced from  $t_{\text{DA}}$  is  $\sim 20$  fs. It is therefore reasonable to consider that the primary  $I$  domain is formed *via* purely electronic processes without structural changes.

After the initial increase of  $\Delta R/R$ , oscillatory structures are observed. By subtracting the baseline of the  $\Delta R/R$  change, we extracted the oscillatory profile  $\Delta R_{\text{OSC}}/R$  [Fig. 2(a) (open circles)]. In Fig. 3(a) (left panel) we

show the Fourier transform of the oscillatory component, in which five peaks are observed. The oscillatory component and the Fourier transform can be well reproduced by the sum of five damped oscillators,

$$\frac{\Delta R_{\text{OSC}}}{R} = \sum_i -A_i \cos(\omega_i t + \phi_i) \exp\left(-\frac{t}{\tau_i}\right) \quad (1)$$

as shown by the solid lines in Figs. 2(a) and 3(a).  $A_i$ ,  $\omega_i$ ,  $\phi_i$ , and  $\tau_i$  are the amplitude, frequency, phase, and decay time of the oscillation  $i$ , respectively. For the  $i = 1$  mode with  $\omega_1 = 53 \text{ cm}^{-1}$ , two decay times (0.19 ps and 5.25 ps) are assumed. The parameter values are listed in Table I. In Fig. 2(a), each oscillation is also shown by solid lines. All the modes are cosine-type, suggesting a displacive-excitation mechanism [12]. All the oscillations have corresponding Raman bands in the  $I$  phase [8,9] and so can be attributed to photogenerated  $I$  domains.

The  $\omega_1$  mode is related to the dimerizations induced by the spin-Peierls mechanism [4], which increase the Coulomb attractive energy in dimers and give rise to additional CT ( $\Delta\rho_1$ ) [Fig. 2(b)]. The other four modes are attributable to the IM totally symmetric ( $a_g$ ) modes [Fig. 2(c)] [10,11]. The modulation of  $\rho$  by such  $a_g$  modes can be explained by the electron-intramolecular vibration (EIMV) coupling [13]: an  $I$  domain initially produced is stabilized by not only dimerizations but also IM deformations. For the  $a_g$  modes of TTF, the IM deformations modulate the molecular orbital energy, leading to the modulation of  $\rho$

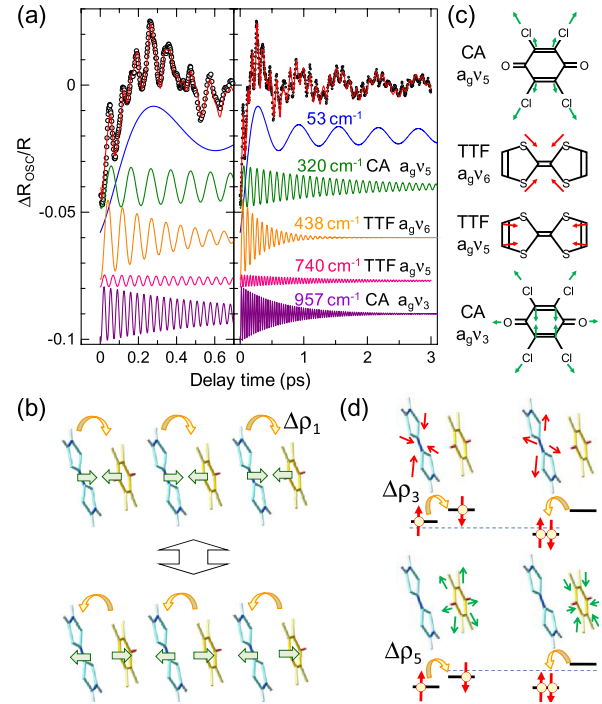


FIG. 2 (color online). (a) Oscillatory component  $\Delta R_{\text{OSC}}/R$ . Solid lines show fitting functions. (b) Oscillations of  $\rho$  by dimeric molecular displacements. (c) IM  $a_g$  modes. (d) Oscillations of  $\rho$  by IM  $a_g$  modes.

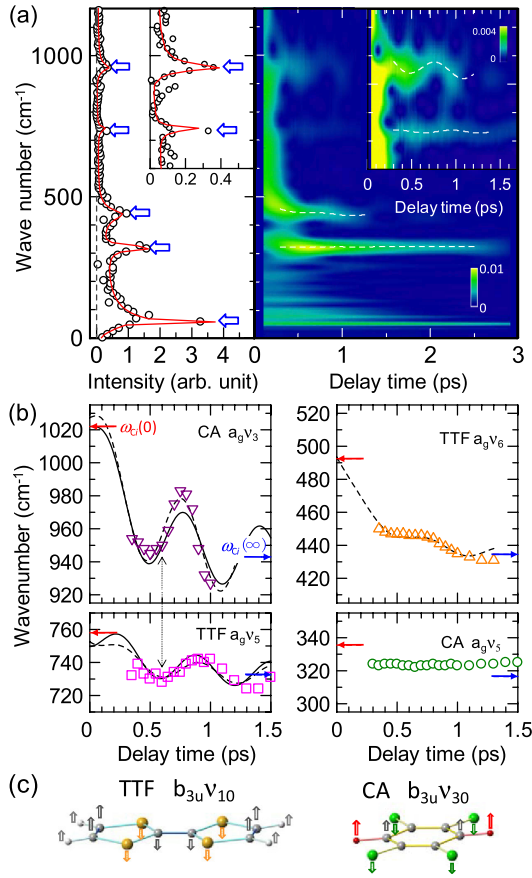


FIG. 3 (color online). (a) Left panel: Fourier transform of the oscillatory component (circles) and the fitting function (solid lines). Right panel: Wavelet transform of the oscillatory component. Broken lines show peaks in Fourier spectra. (b) Time dependence of oscillation frequencies of IM  $a_g$  modes. Broken and solid lines show time profiles calculated using Eq. (2) and Eqs. (3) and (4), respectively. (c) Bending modes.

via the partial CT  $\Delta\rho_i$  between TTF and CA [Fig. 2(d)]. Such deformations give rise to coherent oscillations of molecular structures and  $\rho$ . Similar modulations of  $\rho$  are induced by the  $a_g$  modes of CA. Note that oscillations of  $\rho$  are detected in the IM transition of TTF. The modulation of  $\rho$  in TTF by the vibrations in CA is a clear evidence for the CT process driven by the EIMV coupling.

To obtain quantitative information about the coherent oscillations, we performed wavelet analyses on the oscillatory component and obtained time-dependent Fourier spectra [right panel of Fig. 3(a)] [14]. The frequencies

of some IM oscillations change with time. Their time dependences are plotted in Fig. 3(b). The frequency of CA  $\nu_5$  is almost unchanged, while those of TTF  $\nu_6$ , TTF  $\nu_5$ , and CA  $\nu_3$  are periodically modulated with  $\omega_1 = 53 \text{ cm}^{-1}$  and shift to lower frequencies over time. Modulations of the frequencies are attributable to the modulations of  $\rho$  induced by the dimeric molecular oscillations, while the frequency shifts make us expect the charge redistributions in molecules due to changes of molecular orbitals after the initial  $I$ -domain formation. If the charge redistributions are purely electronic processes, they occur with a time scale ( $\sim 2 \text{ fs}$ ) of overlap integrals ( $\sim 2 \text{ eV}$ ) between neighboring atomic  $\pi$  orbitals. The time constants of the frequency shifts are, however, slow ( $\sim 0.3 \text{ ps}$ ), suggesting that some structural changes might influence the frequency shifts. A plausible scenario is that dimeric molecular displacements give rise to additional IM deformations through vibration couplings, more stabilizing  $I$  states and inducing charge redistributions. Possible candidates for the deformations are bending modes, since both TTF and CA are almost planar in the  $N$  phase and bent in the  $I$  phase [6]. A comparison of the molecular structures in the  $N$  and  $I$  phases as well as theoretical calculations [10,11] revealed the plausible bending modes of TTF ( $b_{3u} \nu_{10}$ ) and CA ( $b_{3u} \nu_{30}$ ) shown in Fig. 3(c), which we label  $j = \alpha$  and  $\beta$ , respectively. The frequencies  $\omega_{Bj}$  of these bending modes are  $\omega_{B\alpha} = 58 \text{ cm}^{-1}$  and  $\omega_{B\beta} = 65 \text{ cm}^{-1}$ .

Next, we analyzed the time dependence of the oscillation frequencies using the following formula:

$$\omega_i(t) = \omega_{Ci}(\infty) + [\omega_{Ci}(0) - \omega_{Ci}(\infty)] \exp\left(-\frac{t}{\tau_{Ci}}\right) - \Omega_i \exp\left(-\frac{t}{\tau_1}\right) \cos(\omega_1 t + \phi_{Ci}). \quad (2)$$

Here,  $\omega_{Ci}(\infty)$  is the frequency in the  $I$  phase (15 K) [9], and  $\omega_{Ci}(0)$  is the frequency in a planar molecule with  $\rho = 0.7$ , evaluated from the frequencies in neutral ( $\rho = 0$ ) and fully ionic ( $\rho = 1$ ) planar molecules [9].  $\tau_1$  is set to be 5.25 ps.  $\tau_{Ci}$  is the time constant for the frequency shift.  $\Omega_i$  and  $\phi_{Ci}$  denote the amplitude and phase of the frequency modulations. The experimental time characteristics are well reproduced by this formula [broken lines in Fig. 3(b)] with three fitting parameters,  $\tau_{Ci}$ ,  $\Omega_i$ , and  $\phi_{Ci}$ . The parameter values are listed in Table I. A notable feature is the variation of phases  $\phi_{Ci}$  in the periodic

TABLE I. Parameters for the analyses of coherent oscillations.

$i$	$\omega_i$ [ $\text{cm}^{-1}$ ]	Assignment	$A_i$ ( $\times 10^2$ )	$\tau_i$ [ps]	$\phi_i$ [deg.]	$\omega_{Ci}(\infty)$ [ $\text{cm}^{-1}$ ]	$\omega_{Ci}(0)$ [ $\text{cm}^{-1}$ ]	$\tau_{Ci}$ [ps]	$\Omega_i$ [ $\text{cm}^{-1}$ ]	$\phi_{Ci}$ [deg.]
1	53	Lattice	3.3 (0.5)	0.19 (5.25)	-3 (7)	-	-	-	-	-
2	320	CA $a_g \nu_5$	0.9	1.52	-18	316.5	335.5	-	-	-
3	438	TTF $a_g \nu_6$	1.7	0.34	-13	434.5	492.5	0.34	3.1	91
4	740	TTF $a_g \nu_5$	0.2	1.25	0	732.5	758	0.3	5.0	-8
5	957	CA $a_g \nu_3$	1.1	0.65	-26	943	1022	0.37	26	98

frequency modulations:  $\varphi_{C4}$  for TTF  $\nu_5$  is almost equal to zero, similarly to the dimeric lattice mode with  $\omega_1 = 53 \text{ cm}^{-1}$ , while for TTF  $\nu_6$  and for CA  $\nu_3$ , the phase shifts ( $\varphi_{C5} = 98^\circ$  and  $\varphi_{C3} = 91^\circ$ ) from the lattice mode are large [see the vertical arrow in Fig. 3(b)].

To clarify the effects of the coupling between the dimeric mode and the bending mode on the frequency changes, we consider a classical oscillator in an external oscillating force expressed as follows:

$$\ddot{Q}_{Bj} + \gamma_{Bj}\dot{Q}_{Bj} + \omega_{Bj}^2 Q_{Bj} = F_{Bj}[1 - \exp(-t/\tau_1)] \times \cos(\omega_1 t). \quad (3)$$

$Q_{Bj}$ ,  $\gamma_{Bj}$ , and  $\omega_{Bj}$  are the vibrational coordinate, damping constant, and frequency of the bending mode  $j = \alpha$  or  $\beta$ , respectively.  $F_{Bj}$ ,  $\tau_1$ , and  $\omega_1$  are the magnitude, the decay time, and the frequency, respectively, of the external force originating from the dimeric molecular displacements. We assume that the photoinduced dimeric displacements expressed as  $Q_1[1 - \exp(-t/\tau_1)\cos(\omega_1 t)]$  induce the bending  $Q_{Bj}(t)$  via Eq. (3).  $Q_1$  shows the dimeric displacement in an  $I$  domain and  $F_{Bj} \propto Q_1$ . We also assume that  $Q_{Bj}(t)$  changes from  $Q_{Bj}(0) = 0$  in the Fran-Condon  $I$  state to  $Q_{Bj}(\infty) \neq 0$  in the lattice-relaxed  $I$  domain and causes a frequency shift of an IM  $a_g$  mode  $i$  from  $\omega_{Ci}(0)$  to  $\omega_{Ci}(\infty)$  through IM charge redistributions. In addition, the dimerization  $[-Q_1 \exp(-t/\tau_1)\cos(\omega_1 t)]$  itself modulates  $\omega_{Ci}(t)$  through the modulation of  $\rho$  as discussed above. Now, we can calculate the time dependence of the frequency  $\omega_{Ci}(t)$  of an IM mode. Assuming that  $\omega_{Ci}(t)$  is linearly dependent on  $Q_{Bj}(t)/Q_{Bj}(\infty)$ ,  $\omega_{Ci}(t)$  is expressed as,

$$\omega_{Ci}(t) = -\bar{\Omega}_i \exp\left(-\frac{t}{\tau_1}\right) \cos(\omega_1 t) + \omega_{Ci}(0) \left[1 - \frac{Q_{Bj}(t)}{Q_{Bj}(\infty)}\right] + \omega_{Ci}(\infty) \frac{Q_{Bj}(t)}{Q_{Bj}(\infty)}. \quad (4)$$

The first term shows the direct modulation of  $\omega_{Ci}(t)$  due to the modulation of  $\rho$  by the dimeric lattice mode, in which the phase is fixed to zero.  $\bar{\Omega}_i$  is the net amplitude of the direct modulation and is different from  $\Omega_i$  (the actual amplitude) in Eq. (2). The second and third terms represent the frequency shifts and modulations by the bending. Using Eqs. (3) and (4), we performed fitting analyses on the time profiles for CA  $a_g\nu_3$  and TTF  $a_g\nu_5$ . The former shows the largest frequency shift and phase shift in the periodic frequency modulation. The latter shows relatively small frequency and phase shifts. The fitting parameters are  $\gamma_{Bj}$  and  $\bar{\Omega}_i$ . The experimental time characteristics were reproduced well [solid lines in left panel of Fig. 3(b)]. The used parameters are  $\gamma_{B\alpha}^{-1} = 0.018 \text{ ps}$  and  $\bar{\Omega}_4 = -8.4 \text{ cm}^{-1}$  for TTF  $a_g\nu_5$ , and  $\gamma_{B\beta}^{-1} = 0.019 \text{ ps}$  and  $\bar{\Omega}_5 = 0 \text{ cm}^{-1}$  for CA  $a_g\nu_3$ . For CA  $a_g\nu_3$ , the direct frequency modulation by the dimeric mode is negligible, and the large frequency change (modulation and shift) and the

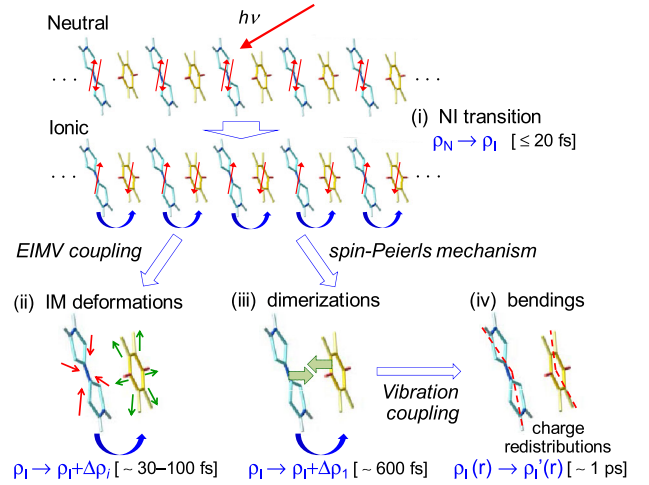


FIG. 4 (color online). Photoinduced NI transition dynamics.

large phase shift are attributable to the large frequency difference [ $\omega_{C5}(0) - \omega_{C5}(\infty)$ ] due to bending and the large damping constant  $\gamma_{B\beta}^{-1}$ .

Finally, we summarize the dynamics in the photoinduced NI transition; see Fig. 4. Just after photoirradiation, an  $I$  domain is generated via purely electronic processes (i). Subsequently, the  $I$  domain is stabilized by molecular deformations (ii) and dimerizations (iii). Simultaneously, changes and coherent oscillations in the degree of CT  $\rho$  due to molecular deformations and dimerizations are generated. The dimerizations produce molecular bendings (iv), which give rise to charge redistributions in molecules. As reported here, in the PIPTs of molecular compounds, changes in the charge and molecular degrees of freedom occur in different time scales, and the system traces a complex transition path. Using information from coherent oscillations, however, it is possible to simulate complicated charge and molecular dynamics.

This work has been partly supported by MEXT, Japan (No. 20110005) and JSPS (No. 20340072).

- [1] For a review, "Photo-induced phase transitions and their dynamics" M. Gonokami and S. Koshihara, *J. Phys. Soc. Jpn.* **75**, 011001 (2006).
- [2] S. Koshihara *et al.*, *Phys. Rev. B* **42**, 6853 (1990).
- [3] E. Collet *et al.*, *Science* **300**, 612 (2003).
- [4] H. Okamoto *et al.*, *Phys. Rev. B* **70**, 165202 (2004).
- [5] J. B. Torrance *et al.*, *Phys. Rev. Lett.* **47**, 1747 (1981).
- [6] M. Le Cointe *et al.*, *Phys. Rev. B* **51**, 3374 (1995).
- [7] J. B. Torrance *et al.*, *Phys. Rev. Lett.* **46**, 253 (1981).
- [8] A. Girlando *et al.*, *J. Chem. Phys.* **79**, 1075 (1983).
- [9] A. Moreac *et al.*, *J. Phys. Condens. Matter* **8**, 3553 (1996).
- [10] C. Katan, *J. Phys. Chem.* **103**, 1407 (1999).
- [11] C. Katan *et al.*, *Phys. Rev. B* **53**, 12112 (1996).
- [12] H. J. Zeiger *et al.*, *Phys. Rev. B* **45**, 768 (1992).
- [13] A. Painelli and A. Girlando, *J. Chem. Phys.* **84**, 5655 (1986).
- [14] H. Suzuki *et al.*, *J. of Acoustic Emission* **14**, 69 (1996).